3
Molecular spectroscopy and dynamics

Formation Mechanism of Multilply-Charged Fullerene Ions

K. Mitsuke, H. Katayanagi, C. Huang, B.P. Kafle, M.S.I. Prodhan, H. Yagi

Division of Chemical. Dynamics and Grad. Univ. Adv. Studies, Inst. for Molec. Sci.,
Myodaiji, Okazaki 444-8585, Japan.

Formation mechanism of multiply-charged fullerene ions was discussed in terms of valence-electron excitation to antibonding unoccupied orbitals and/or spherical standing waves inside the cavity of fullerene. This excitation should be followed by Spectator Auger processes and transmission of the excess electronic energy among enormous vibrational degrees of freedom.

Colavita et al. have calculated the partial photoionization cross sections for valence electrons as a function of $h\nu$ using local density approximation Hamiltonian over an extended energy range. Hence we will discuss the formation mechanism of C_{60}^{2+} from C_{60} with the help of their results. Analogous mechanisms may hold for the formation of C_{70}^{2+} and C_{84}^{2+} from C_{70} and C_{84}, respectively. The partial photoionization cross sections of Colavita et al. were characterized by the presence of many resonances up to about 40 eV above the respective photoionization thresholds. Since the binding energies of five deepest valence orbitals of C_{60} range from -24.2 to -27.5 eV, one can expect that, below $h\nu \sim 65$ eV, these resonances should participate in the formation of C_{60}^{2+}. Among the reported partial cross sections the curve of photoionization of the $3g_g$ and $5h_g$ orbitals demonstrates pronounced broad resonances at $h\nu = 37$ and 50 eV. These resonances are considered to give rise to the peaks at 35 and 50 eV on the cross section curve for double photoionization of C_{60} if we take account of the broadening of the theoretical

peaks by many electron or vibrational effects. Colavita et al. ascribed the resonances at $h\nu = 37$ and 50 eV to promotion of the $3g_g$ and/or $5h_g$ electron to spherical standing waves inside the cavity of fullerene which have high angular momentum. The energies of the final orbitals are calculated from the binding energies (-22.42 and -22.89 eV) of the $3g_g$ and $5h_g$ orbitals to be ~ 14 and ~ 27 eV, corresponding to the resonances at $h\nu = 37$ and 50 eV, respectively.

We can propose a possible pathway for the formation of C_{60}^{2+}, identifying the dominant features of the C_{60}^{2+} cross section curve with the above cavity resonances involving spherical standing waves (see Fig. 1). Let's assume that the cavity-resonance state is formed by promotion of the $3g_g$ or $5h_g$ electron when C_{60} absorbs a 50 eV photon. Then spectator Auger ionization leads to $C_{60}^{+}*$ in which the excited electron is still trapped inside the cavity. This excited state undergoes multiple conversion to nearby cavity- or shape-resonance states by transmitting a part of the electronic energy to numerous vibrational modes. Such conversion may occur consecutively until the excited electron is stabilized down to one of low-lying unoccupied orbitals of antibonding $\sigma*$ or $\pi*$ character near the threshold. Thereby the excess energy of at most ~ 27 eV is dissipated in the fullerene cage. Finally C_{60}^{2+} is produced by tunneling of the electron in the antibonding orbital. We believe this mechanism is most plausible below $h\nu \sim 65$ eV for the formation of C_{60}^{2+}.
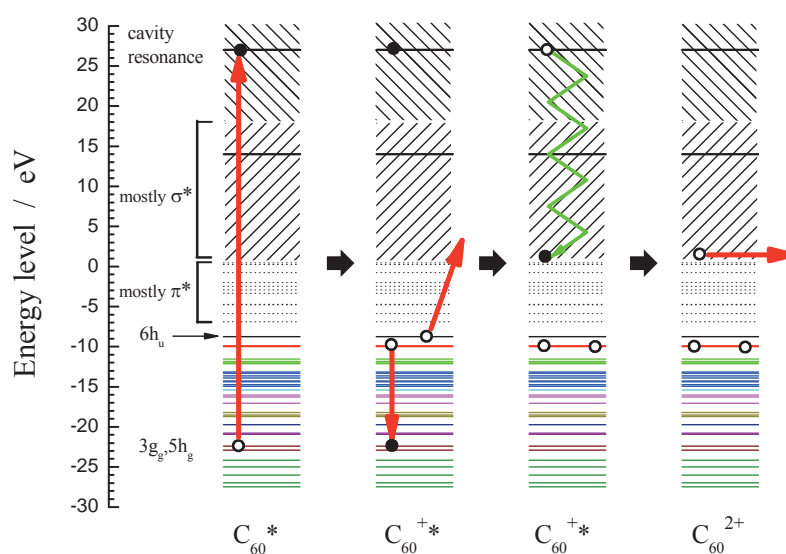
Fig. 1 Schematic picture illustrating the decay mechanism of the cavity-resonance state formed by excitation of the $3g_g$ electron of C_{60}. Vibrationally-excited C_{60}^{2+} can be produced by spectator Auger ionization, multiple internal conversion with intramolecular vibrational redistribution, and tunneling of the excited electron.

Partial Cross Sections for Single and Multiple Photoionization of C_{60}

B.P. Kafle, H. Katayanagi, H. Yagi, M.S.I. Prodhan, C. Huang, K. Mitsuke

Division of Chemical Dynamics and Grad. Univ. Adv. Studies, Inst. for Molec. Sci.,
Myodaiji, Okazaki 444-8585, Japan

Partial cross sections for the photoion formation from C_{60} were determined from the yields of singly-, doubly- and triply-charged ions which were measured by mass spectrometry combined with tunable synchrotron radiation at $h\nu = 25 - 120$ eV.

Open circles of Fig. 1 show the relative partial cross sections $\sigma(C_{60}^{+})$ and $\sigma(C_{60}^{2+})$ for the formation of C_{60}^{+} and C_{60}^{2+} from C_{60}. Each partial cross section includes the contribution of not only the parent but fragment ions produced by the C_2-loss processes, so that it is equal to the cross section involving all the ionic species in a particular charge state. The solid curves in Fig. 1 show partial cross sections for the formation of C_{60}^{+} and C_{60}^{2+} reported by Kou et al. [1], which will be referred to hereafter as $\sigma_{Kou}(C_{60}^{+})$ and $\sigma_{Kou}(C_{60}^{2+})$, respectively. The $\sigma_{Kou}(C_{60}^{+})$ is normalized to $\sigma(C_{60}^{+})$ at $h\nu = 100$ eV. The $\sigma(C_{60}^{2+})$ curve makes a broad maximum at ~50 eV above which it monotonically descends, in consistent with $\sigma_{Kou}(C_{60}^{2+})$ [1]. Nonetheless, $\sigma(C_{60}^{2+})$ is about one third as large as $\sigma_{Kou}(C_{60}^{2+})$ at all photon energies, because, in the present study, we have taken into account the difference in the detection efficiency of C_{60}^{+} and C_{60}^{2+}. The $\sigma(C_{60}^{+})$ and $\sigma_{Kou}(C_{60}^{+})$ curves agree well between 60 and 120 eV. With decreasing $h\nu$ the former curve starts to deviate upwards from the latter curve and the ratio of $\sigma(C_{60}^{+})$ to $\sigma_{Kou}(C_{60}^{+})$ reaches ~2.5 at 25 eV. This discrepancy can be accounted for by that the $\sigma_{Kou}(C_{60}^{+})$ curve has a discontinuity between the $h\nu$ regions covered by grating G2 and that by G3. The contamination of the 2nd-order light of G2 at $h\nu = 40–50$ eV brings about the discontinuity. In the present study correction of the $\sigma(C_{60}^{z+})$ has been performed carefully by estimating the percentage of the 2nd-order light.

Reliability of the present $\sigma(C_{60}^{z+})$ in Fig. 1 can be confirmed by comparing with previously published data of the total photoionization cross section σ_T of C_{60}. In Fig. 2 open circles indicate the sum of $\sigma(C_{60}^{+})$, $\sigma(C_{60}^{2+})$, and $\sigma(C_{60}^{3+})$, which is approximately equivalent to σ_T, while the dotted curve represent the σ_T curve observed by Reinköster et al. [2] and dashed curve does the total photoabsorption cross section calculated by Colavita et al. [3] These three curves are normalized at $h\nu = 100$ eV. Our curve is in a fair agreement with the published curves over a whole energy range, which provides tangible evidence for the validity of our data analysis. Neglecting the m/z-dependence of the detection efficiency resulted in overestimation of $\sigma_{Kou}(C_{60}^{2+})$ and eventually rendered the sum of cross sections, $\sim\sigma_{Kou}(C_{60}^{+})+\sigma_{Kou}(C_{60}^{2+})$ enhanced above 50 eV.

The fine structures observed in $\sigma_{Kou}(C_{60}^{+})$ reappeared in the present $\sigma(C_{60}^{+})$ curve: two peaks at 26 and 34 eV and flat area ranging $40 - 50$ eV. The 34 eV peak was also discernible on the $\sigma(C_{60}^{2+})$ curve as a shoulder. These structures originate from ionization via the shape resonances as single-electron excitation to vacant orbitals. The curve of $\sigma(C_{60}^{3+})$ has an onset around 40 eV and steadily increases with $h\nu$. This onset energy is consistent with the published ionization potential of 35.6 [4] or 39.8 eV [5] for the formation of C_{60}^{3+} from C_{60}.
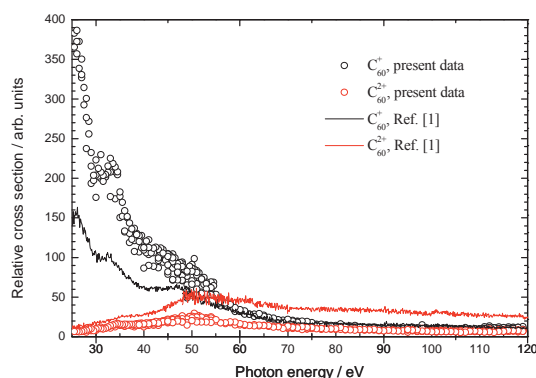
Fig.1 Partial cross sections for single and double photoionization of C_{60}.
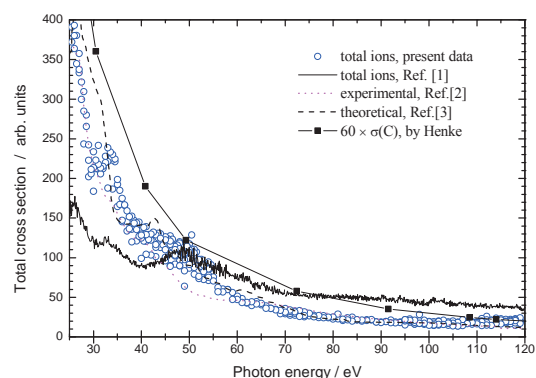
Fig.2 Total photoionization cross section of C_{60}. Comparison between the present and previous data in the literature is made.

[1] Kou et al., J. Chem. Phys. **120** (2004) 6005.
[2] Reinköster et al., J. Phys. B, **37** (2004) 2135.
[3] P. Colavita, et al., Phys. Chem. Chem. Phys. **3** (2001) 4481.
[4] P. Scheier et al., Int. J. Mass Spectrom. Ion Proc. **138** (1994) 77.
[5] Juranic et al., Phys. Rev. A **73** (2006) 04271.

High Resolution Photoelectron Spectroscopy of Gaseous C_{60}

H. Yagi, C. Huang, S. I. Prodhan, B. P. Kafle, H. Katayanagi, K. Mitsuke

Division of Chemical Dynamics and Grad. Univ. Adv. Studies,
Institute for Molecular Science, Okazaki 444-8585 Japan

C_{60} has many degenerate bands in the 7-40 eV ionization energy range. To clarify its electronic structure, photoelectron spectroscopy (PES) studies of solid C_{60} have been made by several groups. However, the PES studies of gaseous C_{60} are few and the energy resolution was about 100 meV at the best, which was not enough to resolve closely spaced bands in detail. We are developing an apparatus of high-resolution angle-resolved PES. Our goal is to carry out PES of various kinds of gaseous fullerenes with a total energy resolution of ~20 meV.

At the beginning, we performed He I (hν=21.2 eV) PES of free C_{60} molecules. The experimental setup is illustrated in Fig. 1. Powder of C_{60} was loaded in a nickel sample holder, which was attached to a conical nozzle, and heated up to 800 K by a cartridge heater. The fullerene vapor was discharged from the nozzle and ionized by He I radiation. Electrons ejected at right angles to the direction of the photon beam were analyzed by the electron energy analyzer (AC-902, comstock). The flux of the fullerene beam was measured by a thickness monitor (XTM/2, Inficon). When the oven temperature was ~800 K, the mass deposition rate was ~16 ng/s. From these values, the number density of C_{60} at the photoionization region is estimated to be 1.2×10^{16} molecules/m^3. The total energy resolution of this apparatus at the pass energy of 3 eV is estimated to be ~50 meV from the peak width of O_2 spectra.

Figure 2 shows the photoelectron spectrum of C_{60} from which the background is already subtracted. The sharp peak at 12.62 eV is attributed to the water contained in the sample powder. Results and experimental conditions of other groups [1,2] are also shown for comparison. Although our data have large uncertainties above ~14 eV due to the large background at low electron kinetic energies, the peak structures below ~14 eV is reconciled well with those of the precedence research. However, in order to elucidate the fine electronic structure such as the Jahn-Teller splitting and the vibrational progressions of C_{60}^+ cations, a better signal to noise ratio is needed. We are now trying to improve S/N ratio by setting the oven unit closer to the ionization region and coating the inner wall of the analyzer by aerodag (a colloidal suspension of fine graphite particles).

As the next step, we plan to carry out PES study at BL2B in UVSOR using a Scienta SES-100 electron spectrometer, which will give higher intensity and better energy resolution. Using BL2B, the partial photoionization cross sections and anisotropy parameters of each band may be determined in the photon energy range of 25-150 eV. The partial cross

sections of the HOMO and HOMO-1 orbitals were reported between 18 and 130 eV photon energies [3], but those of other orbitals are still unknown because their peaks are closely spaced and unresolved.
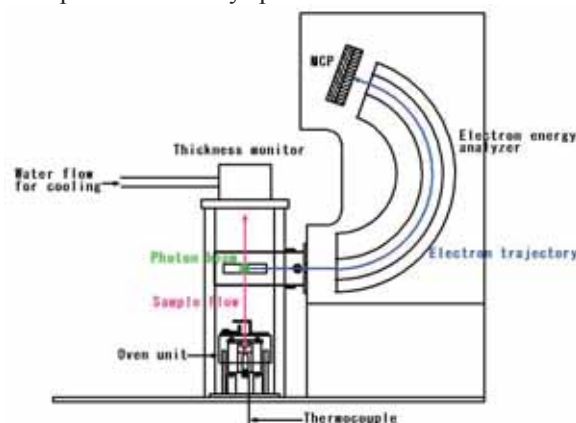
Fig. 1 Apparatus for the photoelectron spectroscopy of gaseous fullerenes. The direction of the photon beam is normal to the paper.
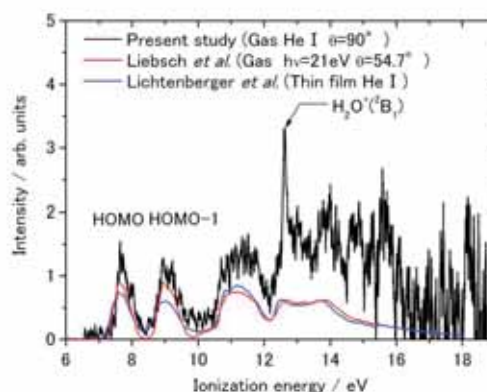
Fig. 2 Photoelectron spectra of C_{60}. The results of other groups are also plotted for comparison [1,2]. θ is the photoelectron sampling angle relative to the photon beam.

[1] T. Liebsch *et al.*, J. Electron Spectrosc. Relat. Phenom. **79** (1996) 419.
[2] D. Lichtenberger *et al.*, Chem. Phys. Lett. **176** (1991) 203.
[3] A. Rüdel *et al.*, Phys. Rev. Lett. **89** (2002) 125503.

Refinements on the Estimation Method of Photoabsorption Cross Sections of Metallofullerenes

H. Katayanagi[1,2], B. P. Kafle[2], T. Mori[1], J. Kou[1],
Y. Takabayashi[3], E. Kuwahara[3], Y. Kubozono[3], K. Mitsuke[1,2]

[1]*Department of Vacuum UV Photo-Science, Institute for Molecular Science, Okazaki 444-8585 Japan*
[2]*Graduate University for Advanced Studies, Okazaki 444-8585 Japan*
[3]*Department of Chemistry, Okayama University, Okayama 700-8530, Japan*

Endohedral metallofullerenes ($M@C_n$; M: metal, n = 60, 70, …) have a unique structure in which one or more metal atoms are encapsulated in a "nano-space" inside a fullerene cage. We carried out a systematic investigation of their absolute photoabsorption cross sections which are expected to be of fundamental importance in various contexts of science and application of metallofullerenes.

We have reported photoabsorption cross sections of several metallofullerenes ($Ce@C_{82}$ [1], $Dy@C_{82}$ [2] and $Pr@C_{82}$ [3]) in the photon energy range available with a monochromator at BL2B in UVSOR. We obtained the values by means of comparison between normalized count rates for the metallofullerenes and standard samples of which cross sections are well known. While the standard samples have much lower masses than those of the metallofullerenes, we did not correct the detection efficiency dependence of the time-of-flight (TOF) mass spectrometer on sample masses and charges at the time. Although the values obtained by our previous study might serve as the first estimate of the cross sections of metallofullerenes, we realized that it was a crude assumption. Accordingly we started an attempt to refine these cross sections.

In the present study, in order to compensate a mass dependence of the detection efficiency we adopted an empirical formula which has been proposed by Twerenbold et al. [4]. The formula gives relative detection efficiency of a Microchannel plate (MCP) detector, which mainly governs the overall detection efficiency of the TOF mass spectrometer. We verified the formula using rare gases (He, Ne, Ar, Kr and Xe) and confirmed that the formula is applicable to our experimental setup.

We applied the formula to our on-going study to evaluate the photoabsorption cross sections of $Pr@C_{82}$ at the outset. In this study, we found out in the photoabsorption spectra that the giant dipole resonance of praseodymium atoms survives regardless of the encapsulation. The refined values for $Pr@C_{82}$ at the on-resonance (130 eV) and off-resonance (110 eV) photon energies are shown in Table 1. In this evaluation we used C_{60} as a standard sample. The cross section at 110 eV agrees well with the cross section (33.5 Mb) 82 times as large as that of a carbon atom $\sigma(C)$. In the previous evaluation without the efficiency correction, the off-resonance value was only approximately 60% of $82\sigma(C)$.

Moreover we measured the phoion yield spectra of Xe in order to use Xe as another standard sample. The cross sections of $Pr@C_{82}$ using Xe as a standard agreed with those using C_{60} as a standard. This agreement shows that the efficiency dependence is fairly corrected.

Without correcting the detection efficiency, we had come to the conclusion that the giant resonance was weakened by the fullerene cage in $Pr@C_{82}$ as well as in $Ce@C_{82}$. In order to ascertain it, we again estimated an enhancement by the giant resonance from the difference between cross sections at 110 and 130 eV. The enhancement was thus 15 Mb, which agreed well with the previous value (16.5 Mb [3]). Similar enhancement by the giant resonance was also observed in $Ce@C_{82}$ [1] and its value was found to be 14.3 Mb. The refined value corroborated our statements that the giant resonance survives but is suppressed by the encapsulation and that it is not specific to $Ce@C_{82}$ but almost universal among metallofullerenes.

In the present study, we confirmed that the absolute values obtained by this method are reliable. Refinements of cross sections for other metallofullerenes as well as higher fullerenes such as C_{70} and C_{84} are also in progress using several standards and the Twerenbold's formula. Accurate determination of cross sections of fullerenes will allow us to assign structures appear in the photoabsorption spectra which arise from molecular nature of fullerenes.

Table 1 Refined cross sections of $Pr@C_{82}$ at the photon energy of 110 and 130 eV. All cross sections are in Mb. Numbers in parentheses show estimated errors.

Photon energy	cross section		
	$Pr@C_{82}^+$	$Pr@C_{82}^{2+}$	Total
110 eV (off-resonance)	22 (11)	15 (4)	37 (12)
130 eV (on-resonance)	28 (11)	24 (7)	52 (13)

[1] K. Mitsuke *et al.,* J. Chem. Phys. **122** (2005) 064304.
[2] K. Mitsuke *et al.,* Int. J. Mass Spectrosc. **243** (2005) 121.
[3] H. Katayanagi *et al.,* UVSOR Activity Report **32** (2006) 51.
[4] D. Twerenbold *et al.,* Proteomics **1** (2001) 66.

Partial Cross Sections for Single and Multiple Photoionization of C_{84}

C. Huang[1], B.P. Kafle[1], H. Katayanagi[1], M.S.I. Prodhan[1], H. Yagi[1],
Y. Kubozono[2], K. Mitsuke[1]

[1]*Division of Chemical Dynamics and Grad. Univ. Adv. Studies, Inst. for Molec. Sci., Myodaiji, Okazaki 444-8585, Japan*
[2]*Dept. of Chem., Okayama Univ., Okayama 700-8530, Japan*

Partial cross sections for the photoion formation from C_{84} were determined from the yields of singly-, doubly- and triply-charged ions which were measured by mass spectrometry combined with tunable synchrotron radiation at $h\nu = 50 – 120$ eV.

The soot containing C_{84} was prepared by an arc-discharge of carbon graphite composite rods with Eu_2O_3. The C_{84} sample was purified by high performance liquid chromatography with toluene as eluent, after a Soxhlet-extraction of the soot. The laser-desorption mass spectrum of the purified sample exhibited only a single peak for C_{84}, and the purified C_{84} sample contains only isomer with D_2 symmetry. About 5 mg of C_{84} was produced with purity better than 99 % from 10 g of the soot.

Figure 1 shows the spectrum taken at $h\nu = 100$ eV, the oven temperature $T = 413$ °C, and mass deposition rate D of 0.2 ng s^{-1}. Peaks of the parent ions C_{84}^{z+} are clearly observed. The shoulder in the smaller m/z side of the main peak of C_{84}^{2+} is ascribed to C_{82}^{2+} and other fragments produced by the C_2-loss processes from C_{84}^{2+}. We calculated the relative partial cross sections $\sigma(C_{84}^{z+})$ ($z = 1 - 3$) for the formation of C_{84}^{z+} from C_{84} in the gas phase that was calculated using

$$\sigma_{abs}(C_{84}^{z+}) \propto R(C_{84}^{z+})\, m\, \overline{v}^2 / \Phi D\, \eta\,(C_{84}^{z+})$$
$$\propto R(C_{84}^{z+})\, T / \Phi D\, \eta\,(C_{84}^{z+}) \equiv \sigma(C_{84}^{z+}),$$

where Φ is the photon flux of synchrotron radiation, and $\eta(C_{84}^{z+})$ is relative detection efficiency of the MCP. The net count rate $R(C_{84}^{z+})$ of the ion signal was computed by integrating the signal counts over each mass peak and then subtracting a uniform background. With increasing photon energy $\sigma(C_{84}^{+})$ shows a slow decrease, while the $\sigma(C_{84}^{3+})$ curve tends to increase gradually. Over the whole $h\nu$ range $\sigma(C_{84}^{2+})$ remains almost flat or slightly declines.

Figures 2 and 3 show the ratio between $\sigma(C_{84}^{2+})$ and $\sigma(C_{84}^{+})$ and that between $\sigma(C_{84}^{3+})$ and $\sigma(C_{84}^{+})$. The ratio $\sigma(C_{84}^{3+})/\sigma(C_{84}^{+})$ has a positive dependence on the photon energy and takes 0.16 at 100 eV. In contrast the $\sigma(C_{84}^{2+})/\sigma(C_{84}^{+})$ curve appears to reach a maximum value of 1.0 around 80 eV and thereafter slowly decreases. The ratios of the partial cross sections are compared with those for C_{60} and C_{70} evaluated at $h\nu \sim 100$ eV. All these ratios can be arranged in descending order as

$$\sigma(C_{70}^{2+})/\sigma(C_{70}^{+})>\sigma(C_{84}^{2+})/\sigma(C_{84}^{+})>\sigma(C_{60}^{2+})/\sigma(C_{60}^{+})$$
and
$$\sigma(C_{70}^{3+})/\sigma(C_{70}^{+})>\sigma(C_{84}^{3+})/\sigma(C_{84}^{+})>\sigma(C_{60}^{3+})/\sigma(C_{60}^{+}).$$
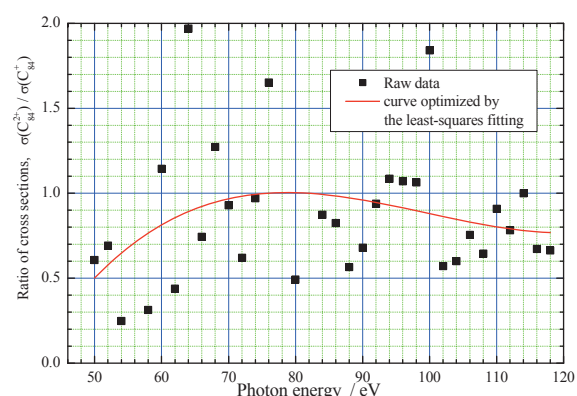
Fig. 2   Ratio between the cross sections for double and single photoionization.

Fig. 1   Time-of-flight mass spectrum of C_{84}.
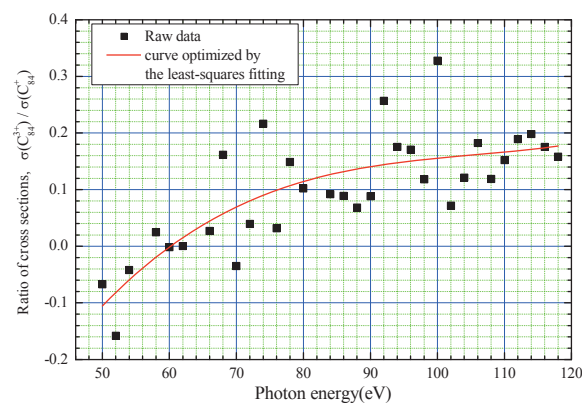
Fig. 3   Ratio between the cross sections for triple and single photoionization.

Observation of Correlation Between Electron Emission and Dissocciation Following S *2p* Excitation of OCS

T. Kaneyasu[1], M. Ito[1,2], Y. Hikosaka[1], E. Shigemasa[1]

[1]UVSOR Facility, Institute for Molecular Science, Okazaki 444-8585 Japan
[2]Graduate School of Science and Technology, Niigata University, Niigata-shi 950-21 Japan

Coincidence detection and correlation analysis among the particles ejected during the relaxation processes of core-excited molecules bring a deeper insight into the molecular inner-shell processes. When both an Auger electron and fragment ions are analyzed in energy, one can give access to the state-to-state dissociation dynamics of the core-excited molecules. We have observed correlation between resonant Auger emission and subsequent molecular dissociation following S $2p_{3/2} \to \pi^*$ excitation of OCS molecules. In contrast to the dipole-allowed direct photoemission from the valence shells, it is expected to observe spin-forbidden states as the Auger final states [1], but their dissociation dynamics has not been revealed.

The experiment was performed on BL4B using the electron-ion coincidence spectrometer [2]. The monochromator bandwidth was set to $E_{ph}/\Delta E_{ph} \sim 1000$ at $h\nu$=164 eV. The electrons ejected at 54.7° with respect to the electric vector of the light were analyzed in energy by the double toroidal electron analyzer, while ions were extracted from the interaction region into the momentum spectrometer by a pulsed electric field according to the electron detection. Arrival positions on the detector and time-of-flights (TOFs) of ions were recorded for every event. The pass energy of the DTA was set to 50 eV for observing resonant Auger electrons in a binding energy range from 14.5 to 19 eV. The resolving power of the DTA was estimated to be $E/\Delta E \sim 50$. The coincidence data set was recorded at $h\nu$=164.3 eV, corresponding to S $2p_{3/2} \to \pi^*$ excitation.

Figure 1 shows a correlation between the resonant Auger final states and the TOFs of the fragments ions. Note that false coincidence events are subtracted. Due to the limited energy resolution in the present setup, the spin-forbidden states are hardly discernible in the electron spectrum. The two bands observed are assigned to the overlap of the $A^2\Pi$ and $B^2\Sigma$ states, and the $C^2\Sigma$ state as noticed in the spectrum. The A and B states are energetically capable to dissociate into $S^+ + CO$, while the C state can decay into both the $S^+ + CO$ and $S + CO^+$ limits. This is roughly confirmed in Fig. 1(a), although the CO^+ fragment is hardly seen in the C state, which may arise from its low branching ratio [3] and the imperfection of the false coincidence subtraction.

We have deduced kinetic energy of the S^+ fragments formed through the dissociations from A, B and C states. In Fig. 2, the energy correlation between the Auger final states and S^+ ions is plotted. Three

dissociation limits of $S^+(^4S) + CO(X^1\Sigma)$, $S^+(^2D) + CO(X^1\Sigma)$ and $S^+(^2P) + CO(X^1\Sigma)$ are energetically accessible, and the limits are indicated by diagonal lines, neglecting the internal energy of CO fragment. The S^+ kinetic energy distributions are spread even to 0 eV, which are due to the vibrational and/or rotational excitations of the neutral CO fragment. The A and B states dissociate into $S^+(^4S, \,^2D) + CO$, while the C state decays into $S^+(^2D, \,^2P) + CO$. The present analysis demonstrates the direct observation of the correlation between the resonant Auger emission and molecular dissociation.
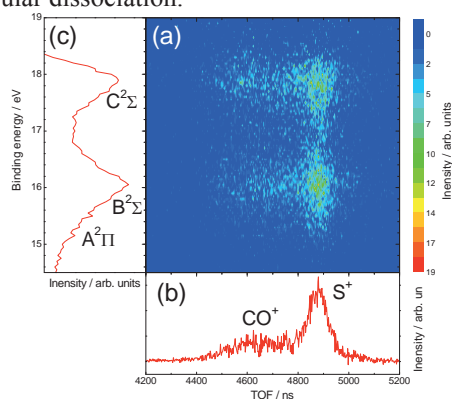
Fig. 1 (a) Correlation between the Auger final states and TOF of fragments. (b) TOF spectrum of fragments. (c) Resonant Auger spectrum.
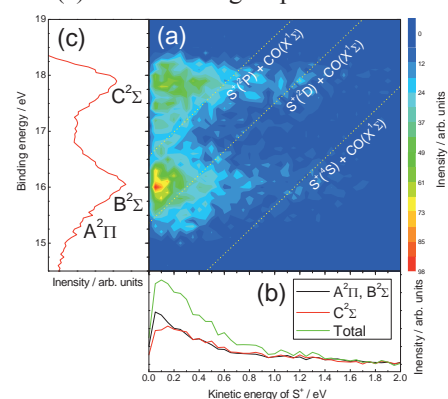
Fig. 2 (a) Correlation between the Auger final states and kinetic energies of S^+ fragments. (b) Kinetic energy distribution of S^+. (c) Resonant Auger spectrum.

[1] S. Masuda *et al*, J. Electron Spectrosc. Relat. Phenom., **137-140** (2004) 351.
[2] T. Kaneyasu *et al*, J. Electron Spectrosc. Relat. Phenom., in press.
[3] S. Morse *et al*., Int. J. Mass Spectrom., **184** (1999) 67.

Three-dimensional Momentum Analyses in Ionic Fragmentations Following Inner-Shell Photoionization

T. Kaneyasu[1], M. Ito[1,2], Y. Hikosaka[1], E. Shigemasa[1]

[1]*UVSOR Facility, Institute for Molecular Science, Okazaki 444-8585 Japan*
[2]*Graduate School of Science and Technology, Niigata University, Niigata-shi 950-21 Japan*

Auger electron-ion coincidence is a powerful method for studying the decay dynamics of core-excited/ionized molecules produced by soft x-ray irradiation. In order to exert the full potential of this method, the spectrometer should be equipped with a performance realizing analyses of vector correlations among the momenta of all the particles emitted. Coincidence imaging spectrometers, which enable to measure three-dimensional momenta of both the electron and ions, have been widely used in the research field of atomic and molecular science. However it becomes difficult to observe fast Auger electrons with a sufficient energy resolution by the imaging technique. In this respect, a conventional electrostatic analyzer is suitable for observing the fast Auger electrons.

We have developed an Auger electron-ion coincidence spectrometer which consists of a double toroidal electron analyzer (DTA) and a three-dimensional ion momentum spectrometer [1,2]. We report on the three-dimensional momentum analysis for fragment ions following the C 1s photoionization of CO. The momentum, energy and angular resolutions for the fragment ions have been evaluated.

The experiment was carried out on BL4B. The DTA pass energy was set to 200 eV for observing the Auger electrons with the binding energy range of 40 – 55 eV. The pulsed electric field for ion extraction was adjusted to ensure the detection angle of 4π sr for ions with kinetic energies less than 6 eV. In this measurement, the arrival positions and time-of-flights (TOFs) of $C^+ + O^+$ ion-pairs were recorded in coincidence with the C 1s Auger spectrum at 334 eV photon energy. Three-dimensional momentum vectors of the ions $\mathbf{P}_1(C^+)$ and $\mathbf{P}_2(O^+)$ are derived from their arrival positions and time information. The momenta of each $C^+ + O^+$ pair should obey the momentum conservation on the two-body fragmentation: $\mathbf{P}_1 + \mathbf{P}_2 = 0$. Conversely, the values of $\mathbf{P}_1 + \mathbf{P}_2$ which are practically observed reflect the momentum resolution of the fragment ions measured by the present spectrometer. Figure 1(a) plots the correlation between $P_{X1} + P_{X2}$ and $P_{Y1} + P_{Y2}$. Here, the x-and y-axes are defined to be perpendicular to the TOF axis, while the z-axis corresponds to the TOF axis which is parallel to the electric vector of the radiation. The spot size on the map reflects the momentum resolution. In order to evaluate the momentum resolution, the sum-momentum distributions are derived by projecting the map onto each axis, which are shown in Figs. 1(b) and 1(c). The peak widths

indicated by arrows in the distributions correspond to momentum resolutions $\sqrt{2}\,\Delta P_{X(Y)}$. As a result we have evaluated momentum resolutions as ΔP_X=11 au, ΔP_Y=17 au. Similarly ΔP_Z=38 au is determined from the $P_{Z1} + P_{Z2}$ distribution. The kinetic energy and angular resolutions are also estimated for the $C^+ + O^+$ events. Figure 2(a) represents the energy difference $3/4 E_1 - E_2$. From the energy spread in the distribution, the energy resolution ΔE is estimated to be 1.3 eV. The angular distribution is analyzed in a similar way to the energy resolution, and the relative angle, $\theta_1 + \theta_2 - 180$, distribution is shown in Fig. 2(b). The emission angle θ is measured with respect to the TOF (electric vector) axis. The angular resolution obtained is better than 18°, which is sufficient to measure the emission angle of the fragment ions and to define initial molecular orientations when the axial-recoil approximation is valid.
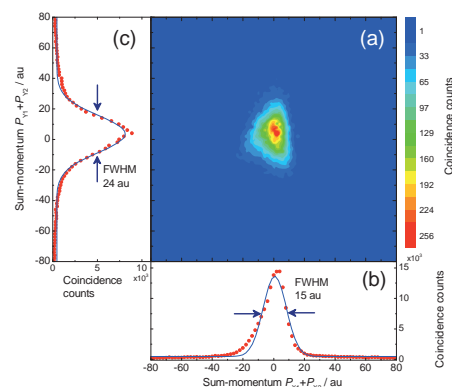
Fig. 1 (a) Contour plot of correlations between the sum-momenta $P_{X1} + P_{X2}$ and $P_{Y1} + P_{Y2}$. Projections of the intensities on the contour plot to (b) x-axis, and to (c) y-axis.
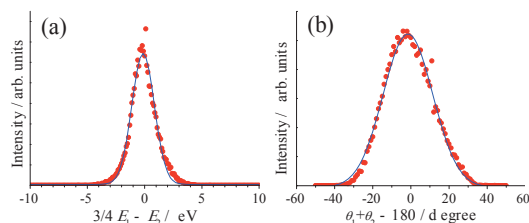
Fig. 2 (a) Energy difference distribution and (b) relative emission angle distribution for the $C^+ + O^+$ dissociation events.

[1] T. Kaneyasu *et al*, AIP conf. proc. **978**, (2007) 1793.
[2] T. Kaneyasu *et al*, J. Electron Spectrosc. Relat. Phenom., in press.

Molecular Deformation of Core-Excited OCS Probed by a Momentum Imaging Method

M. Ito[1,2], T. Kaneyasu[1], Y. Hikosaka[1], K. Soejima[2], E. Shigemasa[1]

[1] *UVSOR Facility, Institute for Molecular Science, Okazaki 444-8585 Japan*
[2] *Graduate School of Science and Technology, Niigata University, Niigata 950-2181 Japan*

Interaction between molecules and soft X-rays is characterized by excitation and ionization of the core electrons. Core-excited molecules decay mostly via Auger electron emission, leading to multiply-charged ion states. The subsequent dissociation of the ion states often results in ionic fragmentations. The emission directions of the fragment ions reflect the molecular structures at the moment of dissociation. An ion momentum correlation measurement, therefore, enables us to determine the molecular structures at the dissociation, and further to discuss the molecular deformations of core-excited states.

In this work, we have studied molecular deformations of core-excited OCS, with an ion momentum spectrometer [1] followed by a position sensitive detector. Here, fragment ions were extracted from an interaction region by a DC electric field, and the momentum vector of each fragment ion was determined from the arrival position on the detector. We have accumulated a multi-ion coincidence dataset at a photon energy of 288 eV which corresponds to the $C1s \rightarrow \pi^*$ resonance. Only the triple coincidences due to the three-body dissociation of OCS^{3+} were used for the present analysis, because this choice enables us to determine directly the momentum vectors of all the fragment ions. The triple coincidences associated with the formation of $O^+ + C^+ + S^+$ can be deduced from the coincidence dataset, by using information on time-of-flight (TOF) differences between the three ion fragments. Fig.1 shows a two-dimensional plot of the numbers of the triple coincidence events, as a function of TOF difference between first hit and second hit (horizontal) and that between first hit and third hit (vertical). The triple coincidences for $O^+ + C^+ + S^+$ can be identified in the marked area.

Figure 2 shows momentum correlations among three ionic fragments included in the triple coincidences. Here, the relative momentum vectors of C^+ and S^+ are plotted, with normalizing the O^+ momentum vectors to $(X,Y)=(-1,0)$. One can see in Fig. 2 that angles between O^+ and S^+ fragments are preferably around 150 degree, while the neutral ground state of OCS has a linear geometry. This observation implies that the molecular geometry is deformed after the inner-shell photoexcitation to OCS $(C1s^{-1}\pi^*)$. Here, a significant molecular deformation is not expected on the OCS^{3+} potential energy surfaces in general, due to the fast dissociation which approximates to the Coulomb explosion. Therefore, the molecular deformation seems to be occurred at OCS $(C1s^{-1}\pi^*)$. The degeneration of OCS $(C1s^{-1}\pi^*)$ is

dissolved by the Renner-Teller effect, and one of the OCS $(C1s^{-1}\pi^*)$ states has a bent geometry. The observed molecular deformation shows a good correspondence to the Renner-Teller distortion at OCS $(C1s^{-1}\pi^*)$.
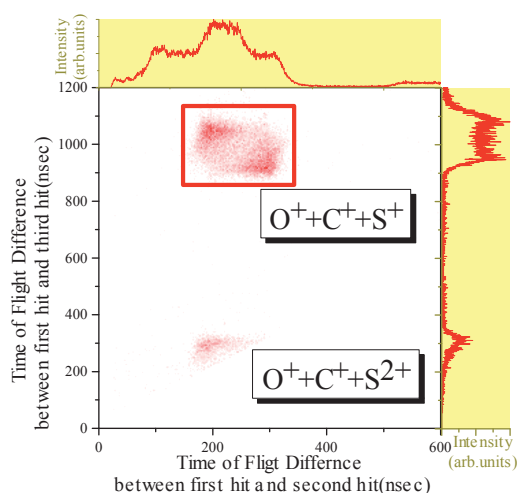
Fig. 1 Time-of-flight difference between first hit and second hit, and those between first hit and third hit. The marked area with a square shows triple coincidences associated with formation of $O^+ + C^+ + S^+$.
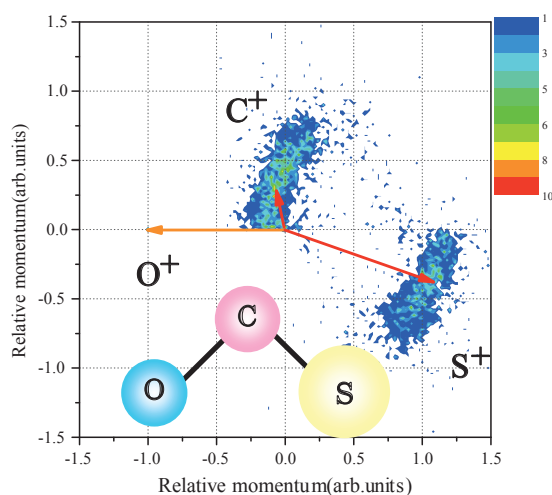
Fig. 2 Momentum correlation for three-body dissociation of OCS^{3+} formed by Auger decay from the $C 1s \rightarrow \pi^*$ resonance.

[1] T. Kaneyasu, Y. Hikosaka, E. Shigemasa, J. Electron. Spectrosc. Relat. Phenom, in press.

Ion Pair Formation in the Vacuum Ultraviolet Region of NO

Y. Hikosaka, T. Kaneyasu, E. Shigemasa

UVSOR Facility, Institute for Molecular Science, Okazaki 444-8585 Japan

Pair formation of positive and negative fragment ions is one of the basic reaction processes induced by interaction between molecules and vacuum ultraviolet photons, though the cross section is highly unfavorable. The cross section of the ion pair formation is often enhanced at neutral excited states, reflecting predissociation of the neutral excited states into ion pair states. The predissociation rate relates to the electronic properties and the potential energy surfaces of the relevant states, and accordingly the neutral excited states which are hardly discernable in the total photoabsorption cross sections may appear remarkably in the cross section for the ion pair formation. Here, one can locate the neutral excited states without direct ionization background, because direct ionization does not contribute to the ion pair formation. The observation of the ion pair formation can be, therefore, a peculiar probe for neutral excited states.

In this work, we have studied the ion pair formation from NO by using a negative ion imaging spectrometer [1]. The advantages of the present imaging method [2] over ordinary mass spectrometry are (i) high collection efficiency (4π-sr. solid angle), and (ii) informativeness on the velocity vector distribution of negative fragment ions. The first useful information derived from the velocity vector distribution is the angular distribution of fragment ions with respect to the electric vector of the incident light. The angular distribution may imply the molecular alignment induced by photoexcitation, where the alignment reflects the symmetries of initially-formed excited states. The kinetic energy distribution of the negative fragment ions is the second useful information derived from the velocity vector distribution, and the internal states of negative and positive fragments are determinable from the kinetic energy distribution. The populations of the final fragment states closely relate to the reaction dynamics.

A negative ion yield curve of NO measured in the photon energy region of 19-25 eV is shown in Fig. 1, in a comparison with a positive ion yield curve. The negative ion yield curve shows much richer structures than the positive ion yield curve. This fact proves the spectroscopic usefulness of negative ion detection to the neutral excited states. Figure 2(a) shows a negative ion image measured at a photon energy of 22.01 eV, where the first two $N^+ + O^-$ limits are accessible. The measured image corresponds to the projection of the three-dimensional velocity distributions for the O^- fragments, where the O^- fragments associated with each $N^+ + O^-$ limit contributes to a circular pattern on the projection,

with intensity concentrated around the circumference. The two rings on the image in Fig. 2(a), which show individual anisotropic intensity distributions with respect to the electric vector, are associated with the first two $N^+ + O^-$ limits. Figure 2(b) shows a transformed image using an onion-peeling procedure. On the transformed image, obviously the two rings corresponding to the individual $N^+ + O^-$ limits become clearer than those on the image in Fig. 2(a). The total intensity of each ring gives the population of the corresponding final $N^+ + O^-$ pair, and the intensity distribution along the ring shows the angular distribution relative to the electric vector.
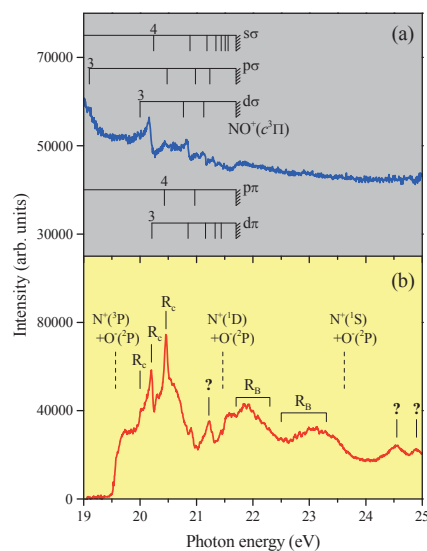
Fig. 1 (a) Positive ion yield curve and (b) negative ion yield curve of NO. R_c and R_B denote Rydberg states converging to $NO^+(c^3\Pi)$ and $NO^+(B^1\Pi)$, respectively.
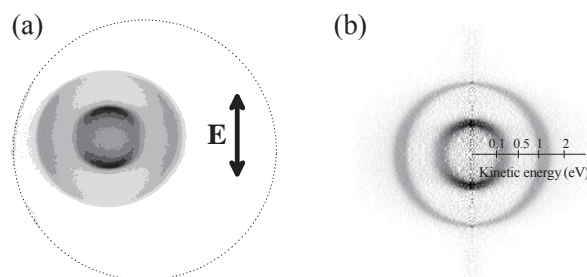
Fig. 2 (a) Negative ion image measured at a photon energy of 22.01 eV, where the first two ion pair limits are accessible. (b) Transformed image using an onion-peeling procedure.

[1] Y. Hikosaka, T. Kaneyasu and E. Shigemasa, J. Electron Spectrosc. Relat. Phenom. **154** (2007) 43.
[2] Y. Hikosaka and E. Shigemasa, J. Electron Spectrosc. Relat. Phenom. **148** (2005) 5.